Rapid Communications

Role of particle orientational order during shear thickening in suspensions of colloidal rods

Vikram Rathee,[1,2,*] Srishti Arora,[3] Daniel L. Blair,[2] Jeffrey S. Urbach,[2] A. K. Sood,[1,3,†] and Rajesh Ganapathy[3,4,‡]

[1]*Department of Physics, Indian Institute of Science, Bangalore 560012, India*

[2]*Department of Physics and Institute for Soft Matter Synthesis and Metrology, Georgetown University, Washington, D.C. 20057, USA*

[3]*International Centre for Materials Science, Jawaharlal Nehru Centre for Advanced Scientific Research, Jakkur, Bangalore 560012, India*

[4]*School of Advanced Materials (SAMat), Jawaharlal Nehru Centre for Advanced Scientific Research, Jakkur, Bangalore 560064, India*

(Received 8 October 2019; revised manuscript received 21 January 2020; accepted 11 March 2020; published 6 April 2020)

Rheology of dense anisotropic colloidal suspensions often exhibits unsteady flow at constant imposed shear stress and/or shear rate. Using simultaneous high-resolution confocal microscopy and rheology, we find that the temporal behavior arises due to a strong coupling between shear flow and particle orientation. At smaller applied stresses, the orientation of rods fluctuates around the flow direction. A transition to an intermittent disordered state is observed at higher stresses when the angle between the flow and the rod orientation reaches a critical value. This disordered state is associated with transient drop in shear rate and an increase in viscosity. Simultaneous visualization of boundary stresses and orientation shows that the disordered regions lead to heterogeneous stresses and positive normal forces at the boundary, indicating the formation of systems spanning disordered particle contact networks.

DOI: 10.1103/PhysRevE.101.040601

When subjected to shear stresses beyond a material-dependent threshold value, most dense suspensions shear thicken; their viscosity η increases with the stress σ [1–3]. Recent studies suggest that while the hydrocluster mechanism [4,5] can account for a modest increase in η, a larger increase stems from particles forming a stress-induced frictional contact network [6–13]. These studies are limited to mainly spherical or compact particles, despite the fact that altering the particle shape greatly affects rheological response [14–16]. It has been shown that an increase in the particle aspect ratio, α, reduces the volume fraction (ϕ = total particle volume / total system volume) at which shear thickening sets in [16,17]. Previous small-angle neutron scattering (SANS) measurements of suspensions of elongated particles in the shear-thickening regime indicated that particle flow alignment was retained in the shear-thickened state [15]. Since scattering approaches are inherently ensemble-averaged measurements, these do not capture changes in local orientational order. These concerns notwithstanding, the strong coupling between flow and particle shape anisotropy is known to result in rich time-dependent flows [14,18,19]. A complex temporal behavior has in fact been observed during shear thickening in both Brownian and non-Brownian suspensions of spherical [6,13] or compact particles [20,21], highlighting the importance of investigating temporal dynamics of orientable particles during shear thickening.

In this Rapid Communication, we investigate the mechanism of shear thickening in colloidal rod suspensions by direct imaging of particle orientational order under shear and spatially resolved boundary stress measurements [22]. Our key results are that shear thickening in these systems is primarily an outcome of the rich interplay between fluctuations in particle orientational order and the formation of gap spanning contact networks.

We synthesized colloidal silica rods following the procedure first developed by Kuijk *et al.* [23]. We obtained the rods having a typical diameter $d = 400$ nm and length of $l = 4\ \mu$m ($\alpha \equiv l/d \sim 10$) (see the Supplemental Material, Sec. S1 [24]). The particles were dispersed in a glycerol-water mixture (85% glycerol by volume) at different ϕs and η was measured as a function of σ in a cone-plate geometry on a stress-controlled rheometer (AntonPaar, Austria). We varied ϕ from 0.19 to 0.45 where the suspensions form a nematic phase in equilibrium and the flow response is typical of shear-thickening particulate suspensions (Fig. 1(a)) [12]. On increasing σ, the suspensions shear thin and reach a viscosity plateau, $\eta_N(\phi)$. This plateau persists up to an onset stress σ_c beyond which the suspensions shear thicken. Like in suspensions of spherical particles [11,12], and in a recent study on shear jamming in colloidal rods [25], we also found σ_c to be approximately independent of volume fraction ϕ [Fig. 1(a)]. At even larger stresses, η almost plateaus to a constant value that corresponds to the viscosity of the shear-thickened state, $\eta_{ST}(\phi)$. In the shear-thickening regime, $\eta \propto \sigma^{\beta}$, where the shear-thickening exponent β is positive and steadily grows with ϕ but remains below unity (continuous shear thickening) for $0.19 \leqslant \phi < 0.38$. However, for $\phi \geqslant 0.38$, $\beta = 1$, i.e., the suspension viscosity increases at a fixed shear rate, $\dot{\gamma}$, which is a characteristic of discontinuous shear thickening (DST). Remarkably, our suspensions show shear thickening at particle loadings that are substantially smaller than those required for isotropic particles ($\beta > 0$ even for $\phi = 0.19$).

*vi21@georgetown.edu
†asood@iisc.ac.in
‡rajeshg@jncasr.ac.in

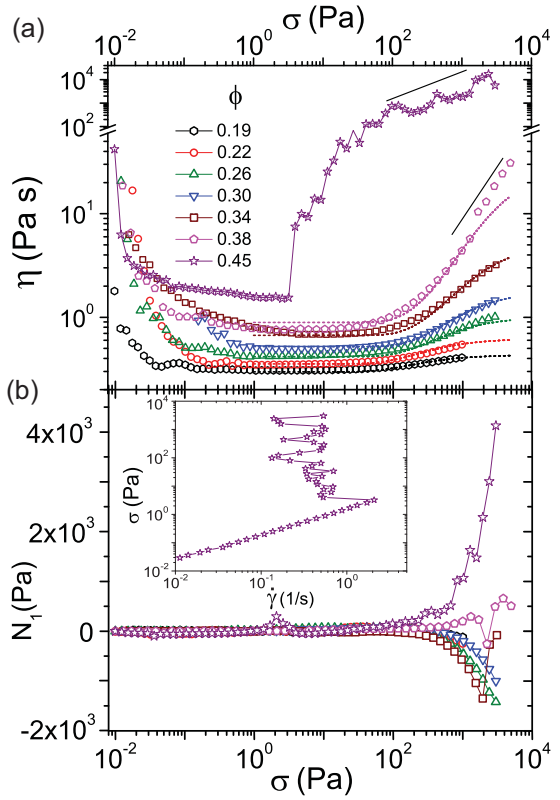

FIG. 1. (a) Flow curves and (b) first normal stress difference N_1 at various ϕs, for colloidal rods of aspect ratio $(\alpha) \equiv l/d \sim 10$. The dotted lines in panel (a) are fit to $\eta(\sigma, \phi) = [1 - \phi/\phi_c(\sigma)]^{-2}$, where $\phi_c(\sigma) = f\phi_m + (1-f)\phi_o$, f is the fraction of frictional contacts, and ϕ_o and ϕ_m correspond to viscosity divergences for purely frictionless and frictional contacts, respectively. Inset (b) shows σ vs $\dot{\gamma}$ at $\phi = 0.45$.

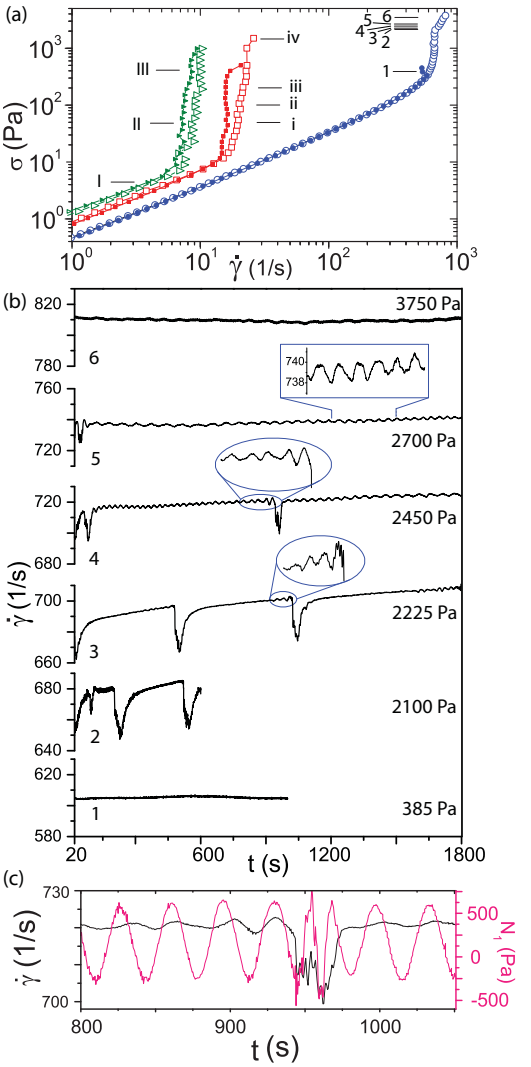

FIG. 2. (a) Flow curves for $\phi = 0.36$ (blue circles), $\phi = 0.4$ (red squares), and $\phi = 0.42$ (green triangles) samples. Forward and reverse stress sweeps are shown by hollow and solid symbols, respectively. The stress values at which shear-rate relaxation measurements were carried out are indicated on the flow curves. (b) Shear rate relaxation, i.e., time dependence of shear rate, $\dot{\gamma}$, at various σs for $\phi = 0.36$. The panel numbers in panel (b) correspond to those indicated in flow curve [blue circles in panel (a)]. (c) $\dot{\gamma}$ (black line) and N_1 (dark pink line) for $\sigma = 2450$ Pa. The data correspond to the highlighted region in panel 3 in Fig. 2(b).

This dependence on β with ϕ is consistent with earlier reports on similar system [25], which find that the larger effective excluded volume of anisotropic particles [26–28] in comparison to isotropic ones aid in achieving shear thickening even at low volume fractions. The behavior of $N_1(\sigma)$ at various ϕs is similar to that seen in Ref. [12] [Fig. 1(b)]. For $\phi < 0.34$, N_1 hovers around zero for small applied stresses and turns negative beyond σ_c, indicating dominating hydrodynamic forces. However, at $\phi = 0.34$, N_1 first becomes increasingly negative above σ_c, but abruptly changes sign and becomes more positive for $\sigma \geqslant 2000$ Pa, due to dominating contact forces [Fig. 1(b), open squares]. On increasing ϕ, N_1 becomes positive beyond σ_c [Fig. 1(b), open pentagons and open stars]. While the observed behavior of N_1 with increasing ϕ is similar to suspensions of spheres, we note that the algebraic sign of N_1 is not always directly indicative of the presence of frictional contact networks. Experiments on non-Brownian particles, where frictional interactions are known to be dominant [29], have observed a negative N_1 during shear-thickening [30,31].

Fluids that show DST often have an S-shaped flow curve [32] with an intermediate region where $d\sigma/d\dot{\gamma} < 0$ [Fig. 1(b) inset]. Since homogeneous flow is impossible in these regions, the system behaves heterogeneously, through the formation of shear bands. In many complex fluids, the canonical example being shear-thinning wormlike micellar gels [33–35], the bands themselves can become unstable and can exhibit *rheochaos*—time-dependent flows at fixed σ or $\dot{\gamma}$ at Reynold's number Re $<<$ 1 [36]. In dense Brownian as well as non-Brownian suspensions, the flow is unsteady [6,13,37] and exhibits rheochaos in the DST regime [20,21,38,39]. Such complex flow response is not captured by the mean-field Wyart and Cates (WC) model. Motivated by these findings, we set out to ascertain if bulk flow in the DST regime [stars in Fig. 1(a)] was unstable.

Accordingly, we carried out shear rate relaxation measurements at various imposed stresses. Figure 2(a) shows forward (hollow symbols) and reverse (solid symbols) flow curves

for $\phi = 0.36 < \phi_m$ (circles), $\phi = 0.4 \approx \phi_m$ (squares), and $\phi = 0.42 > \phi_m$ (triangles), respectively. Figure 2(b) summarizes the complex dynamics observed for few representative stresses. When $\sigma \approx 400$ Pa, where the flow curve is single valued, $\dot{\gamma}$ is approximately constant [Fig. 2(b), panel 1]. For regions of the flow curve where the stress is multivalued [Fig. 2(b), panels 2–5], $\dot{\gamma}$ shows rich temporal dynamics. At $\sigma = 2100$ Pa, $\dot{\gamma}$ first increases and then saturates before rapidly dropping close to its original value. This behavior is cyclic. On increasing σ [Fig. 2(b), panels 3–5], not only does the cycle duration increase substantially but also we see small-amplitude oscillations preceding the drop in $\dot{\gamma}$. As the drop in $\dot{\gamma}$ is approached, the amplitude of the oscillations grows and their frequency increases. Most remarkably, oscillations in $\dot{\gamma}$ are also well correlated with those in N_1 [Fig. 2(c)]. The time period of the oscillations ($\approx$25 s) is much larger than the rotational time period of the cone ($\approx$0.5s) and inertial time period ($\approx$ 0.2s), indicating these are not an outcome of instrument imperfections [20]. At even larger σs [panel 6 in Fig. 2(b)], where the flow curve is once again single valued, the time dependence entirely vanishes.

To gain microscopic insights into these observations, we tracked the dynamics of rods using a confocal rheometer [40,41]. The sample was doped with a small amount of fluorescently labeled rods [42] for determining the local orientation. Under shear, we estimated the angle $\bar{\theta}$ between the average orientation of rods, $\hat{n}$, in the field of view with respect to the flow direction $\mathbf{v}$, by calculating the distribution of local orientation in each image (see the Supplemental Material [24] for details).

Owing to the very high particle velocities in the ST regime for the $\phi = 0.36$ sample, particles could not be tracked. Thus, we increased ϕ to 0.4, where $\sigma_c \approx 10$ Pa and the $\dot{\gamma}$ values during DST are substantially smaller [Fig. 2(a)]. We also observed hysteresis during the forward and reverse stress sweeps [Fig. 2(a), squares]. For $\sigma = 30$ Pa ($> \sigma_c$), we observed stable oscillations in $\bar{\theta}$ with a clear correlation between $\bar{\theta}$ and $\dot{\gamma}$, where both quantities fluctuate between two limiting values, as shown in Fig. 3(a) (see the Supplemental Material [24], movie S1). Surprisingly, when $\bar{\theta}$ is positive, i.e., when average orientation of the rods is toward the free surface, $\dot{\gamma}$ is higher. A gradual decrease in $\bar{\theta}$ toward negative values (rod orientation toward $-\nabla \times \mathbf{v}$) is accompanied by a decreases in $\dot{\gamma}$. The correlation between the orientation, which is determined from a small region of the sample, and the average rheological response suggests that the orientation oscillations occur coherently throughout the sample. At $\sigma = 100$ Pa, along with oscillations, we observed intermittent disordered regions represented by an instantaneous jump in $\bar{\theta}$ [Fig. 3(b)]. A representative snapshot corresponding to this state [Fig. 3(f)] shows a substantial number of rods oriented along the ∇v direction (seen as circles since the rod orientation is perpendicular to imaging plane) and many rods also tilted toward the vorticity direction. The orientation changes occur when an order-disorder transition either takes place in the field of view or a disordered region is advected into the field of view. At $\sigma = 200$ Pa, the oscillations in $\bar{\theta}$ are more pronounced and occur for longer duration. Remarkably, this abrupt transition occurs when $\bar{\theta}$ reaches a critical negative angle [Fig. 3(c) and Supplemental Material, movie S2]. As

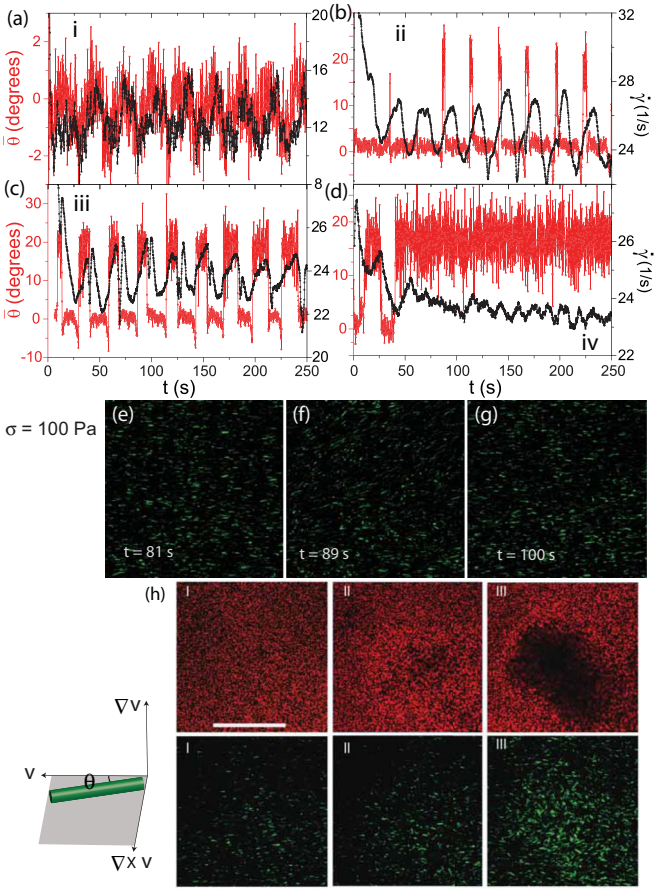

FIG. 3. [(a)–(d)] Time dependence of $\dot{\gamma}$ (black symbols) and the angle $\bar{\theta}$ between S and $\mathbf{v}$ (red symbols) at various σs for $\phi = 0.4$. (a) $\sigma = 30$ Pa. (b) $\sigma = 100$ Pa. (c) $\sigma = 200$ Pa. (d) $\sigma = 1100$ Pa. Panels (a), (b), (c), and (d) correspond to points labeled (i), (ii), (iii), and (iv) on the flow curve, respectively [Fig. 2(a)] (red squares). Snapshots of tracer rods at $\sigma = 100$ Pa [Fig. 3(b)] at times when $\bar{\theta}$ is (e) small (and negative), (f) large and positive at the beginning of disordered region, and (g) small (and positive) when the order is restored again. (h) Simultaneous boundary stress microscopy and confocal imaging of rod orientations during flow curve measurements at $\phi = 0.42$. The top panels are images of fluorescent colloids attached to a elastic substrate (bottom plate) and correspond to different stress values along the flow curve for $\phi = 0.42$ [Fig. 2(a), green triangles]. Bottom panels are the corresponding images of tracer rods. (I) $\sigma = 5$ Pa, (II) $\sigma = 50$ Pa, and (III) $\sigma = 400$ Pa. Black regions in panel (h) appear when the elastic substrate is pushed down due to large normal stresses, which results in these regions going out of focus. Scale bar: 70 μm. The inset shows a sketch of coordinate system in three dimensions.

is also apparent in movie S2, there is a coupling between the rod orientation and nonaffine flow, with the rod orientation indicating the local flow direction. For $\sigma = 1100$ Pa, where the flow curve is almost single valued, the amplitude of oscillations in $\dot{\gamma}$ are considerably smaller, with the dynamics in $\dot{\gamma}$ and $\bar{\theta}$ appearing noisy [Fig. 3(d) and Supplemental Material, movie S3]. However, before reaching this steady state, $\bar{\theta}$ first dropped to a negative value and then jumped to a large positive value similar to $\sigma = 200$ Pa. Note that in the disordered state, the determination of $\bar{\theta}$ is not straightforward, but the algorithm

produces a robust positive value (Figs. 3(b)–3(d) and the Supplemental Material).

There are a number of surprising aspects to the behavior described above. The existence of a positive angle at low ϕ (Supplemental Material [24], Fig. S5 and movie S4) represents an asymmetry that is not present in simple shear, where there would be no preference for positive versus negative deflection. However, the shear geometry here has a free surface and curved flow lines even for affine flow. It has been observed that anisotropic particles under shear are often tilted in the positive $\dot{\gamma}$ direction as a result of shear-induced interparticle interactions [43–45] and some similar mechanism may be at play here. At higher concentrations, the tilt is suppressed and replaced by collective oscillations about $\theta = 0$, that are accompanied by oscillations in $\dot{\gamma}$ and $\hat{n}$ [Fig. 3(a)]. As the angle varies from zero in either direction, the degree of alignment reduces and when orientations exceed a critical negative $\bar{\theta}$ it results in unstable flow and the formation of disordered particle clusters above σ_c (Fig. 3). In our case, we do not observe unstable state if the angle is positive, possibly due to the presence of a free surface. Similar behavior is observed in a parallel-plate geometry for $\phi = 0.39$ (DST regime) and also for different background solvent viscosity, suggesting that these findings are intrinsic to the suspension rheology and do not depend on rheometer inertial time as observed by Hermes *et al.* (see the Supplemental Material [24] and Figs. S6– S10) [20].

To determine if particle orientational disorder in the DST regime results in a positive N_1 and locally higher shear stresses, we employed a technique known as boundary stress microscopy (BSM), which provides spatiotemporal information of normal and shear forces [13,46,47]. Here, we covalently attached fluorescent microspheres to a polydimethylsiloxane (PDMS) layer of known elasticity bonded to a glass coverslip that serves as bottom boundary of the sample in the confocal rheometer (see the Supplemental Material [24]). The out-of-plane motion of the beads, i.e., along ∇v, provides information about local normal stresses. Regions of high N_1 generate out-of-plane motion of the microspheres, resulting in dark patches in the images as particles move out of the confocal imaging plane. During ST in suspensions of colloidal spheres, stress heterogeneities at the boundary indicate the existence of transient gap-spanning particle contact networks [13]. The top and bottom panels in Fig. 3(h) show images of the spheres on bottom surface and tracer rods just above this surface, respectively, for various applied σs labeled (I)–(III) on the flow curve for $\phi = 0.42$ [triangles in Fig. 2(a)]. When $\sigma < \sigma_c$, the rods are flow aligned and stress heterogeneities are absent [all beads appear in focus in Fig. 3(h), panel (I)]. For $\sigma = 50$ Pa $> \sigma_c$, the beads intermittently appear slightly out of focus and the rod orientation above this region appear slightly disordered [Fig. 3(h), panel (II)]. At even larger stresses, the beads move completely out of the imaging plane, as the orientationally disordered region pushes down on the elastic substrate [Fig. 3(h), panel (III), $\sigma = 400$Pa, and the Supplemental Material [24], movie S5]. As can be seen in the movie, these disordered regions are associated with a local increase in the flow velocity. With increasing σ, we observed a concomitant increase in the frequency of these regions of large local displacement. The out-of-focus movement of beads is an indication of positive normal forces (F_N) and in cone-plate geometry $N_1 = F_N/$(plate area). An increased frequency and amplitude of heterogeneous stresses indicate that N_1 increases with applied stress and is in good agreement with the increase in N_1 observed in flow curve measurements in Fig. 1(b). Further, the combination of confocal-rheology and BS measurements clearly show that the coupling of particle orientation to shear and normal stresses plays a prominent role in the shear thickening (ST) of anisotropic particles and stands in contrast to findings from previous Rheo-SANS measurements [15].

The collective picture which emerges from our study is that shear thickening even in suspensions of anisotropic particles has its origins in particles forming a disordered contact network, as evident in particle imaging and boundary stress measurements. It seems surprising at first that rods of large-aspect-ratio shear thicken at relatively lower volume fractions than spheres despite the fact that these can pack more densely in a shear-aligned state. However, it is known that anisotropic particles can from more contacts in a disordered state, resulting in jamming at a volume fraction that decreases with increasing aspect ratio [27]. The coupled oscillations in average orientation, suspension viscosity, and normal stress that we observe are similar to those observed in other rod suspensions [14,18,19]. In general, the degree of orientational order is coupled with the flow alignment, and we speculate that as the magnitude of $\bar{\theta}$ becomes large, the degree of order decreases, resulting in an increase in high-stress particle collisions, producing frictional interactions and an instability to the fully disordered, shear jammed state.

Acknowledgments. We thank Prof. Peter Olmsted for helpful discussions. This work was in part supported by the National Science Foundation (Grant No. ENG-1907705). A.K.S. thanks the Department of Science and Technology (DST), Government of India, for a Year of Science Fellowship. R.G. thanks ICMS, SAMat, and JNCASR for support.

[1] H. A. Barnes, J. Rheol. **33**, 329 (1989).
[2] N. J. Wagner and J. F. Brady, Phys. Today **62**(10), 27 (2009).
[3] E. Brown and H. M. Jaeger, Rep. Prog. Phys. **77**, 046602 (2014).
[4] D. R. Foss and J. F. Brady, J. Fluid Mech. **407**, 167 (2000).
[5] X. Cheng, J. H. McCoy, J. N. Israelachvili, and I. Cohen, Science **333**, 1276 (2011).
[6] D. Lootens, H. van Damme, Y. Hemar, and P. Hebraud, Phys. Rev. Lett. **95**, 268302 (2005).
[7] N. Fernandez *et al.*, Phys. Rev. Lett. **111**, 108301 (2013).
[8] R. Seto, R. Mari, J. F. Morris, and M. M. Denn, Phys. Rev. Lett. **111**, 218301 (2013).
[9] M. Wyart and M. E. Cates, Phys. Rev. Lett. **112**, 098302 (2014).
[10] N. Y. C. Lin, B. M. Guy, M. Hermes, C. Ness, J. Sun, W. C. K. Poon, and I. Cohen, Phys. Rev. Lett. **115**, 228304 (2015).
[11] B. M. Guy, M. Hermes, and W. C. K. Poon, Phys. Rev. Lett. **115**, 088304 (2015).

[12] J. R. Royer, D. L. Blair, and S. D. Hudson, Phys. Rev. Lett. **116**, 188301 (2016).
[13] V. Rathee, D. L. Blair, and J. S. Urbach, Proc. Natl. Acad. Sci. USA **114**, 8740 (2017).
[14] P. M. Lettinga, Z. Dogic, H. Wang, and J. Vermant, Langmuir **21**, 8048 (2005).
[15] R. G. Egres and N. J. Wagner, J. Rheol. **49**, 719 (2005).
[16] E. Brown, H. Zhang, N. A. Forman, B. W. Maynor, D. E. Betts, J. M. DeSimone, and H. M. Jaeger, Phys. Rev. E **84**, 031408 (2011).
[17] Y. Ye *et al.*, ACS Appl. Nano Mater. **1**, 2774 (2018).
[18] V. Faraoni, M. Grosso, S. Crescitelli, and P. L. Maffettone, J. Rheol. **43**, 829 (1999).
[19] M. Grosso, S. Crescitelli, E. Somma, J. Vermant, P. Moldenaers, and P. L. Maffettone, Phys. Rev. Lett. **90**, 098304 (2003).
[20] M. Hermes *et al.*, J. Rheol. **60**, 905 (2016).
[21] B. Saint-Michel, T. Gibaud, and S. Manneville, Phys. Rev. X **8**, 031006 (2018).
[22] Some of the key findings from this study were first presented at the KITP Conference on "Non-linear mechanics and rheology of dense suspensions: Nanoscale structure to macroscopic behavior" held in January 2018 and are available online at http://online.kitp.ucsb.edu/online/suspensions_c18/sood/.
[23] A. Kuijk, A. van Blaaderen, and A. Imhof, J. Am. Chem. Soc. **133**, 2346 (2011).
[24] See Supplemental Material at http://link.aps.org/supplemental/10.1103/PhysRevE.101.040601 for details about sample preparation and boundary stress microscopy measurements, fitting to the model of Ref. [9], and the calculation of orientation angle, as well as data on orientation dynamics at different temperatures and gaps in the parallel pate geometry.
[25] N. M. James, H. Xue, M. Goyal, and H. M. Jaeger, Soft Matter **15**, 3649 (2019).
[26] L. Onsager, Ann. N.Y. Acad. Sci. **51**, 627 (1949).
[27] A. P. Philipse, Langmuir **12**, 1127 (1996).
[28] C. Ferreiro-Cordova and D. S. van Duijneveldt, J. Chem. Eng. Data **59**, 3055 (2014), and references therein.
[29] S. Gallier, E. Lemaire, F. Peters, and L. Lobry, J. Fluid Mech. **757**, 514 (2014).
[30] A. Singh and P. R. Nott, J. Fluid Mech. **490**, 293 (2003).
[31] Z. Pan, H. de Cagny, M. Habibi, and D. Bonn, Soft Matter **13**, 3734 (2017).
[32] Z. Pan, H. de Cagny, B. Weber, and D. Bonn, Phys. Rev. E **92**, 032202 (2015).
[33] R. Bandyopadhyay, G. Basappa, and A. K. Sood, Phys. Rev. Lett. **84**, 2022 (2000).
[34] R. Ganapathy and A. K. Sood, Phys. Rev. Lett. **96**, 108301 (2006).
[35] R. Ganapathy and A. K. Sood, J. Non-Newton. Fluid **149**, 78 (2008).
[36] P. D. Olmsted, Rheol. Acta **47**, 283 (2008).
[37] V. Rathee, D. L. Blair, and J. S. Urbach, J. Rheol. **64**, 299 (2020).
[38] M. Grob, A. Zippelius, and C. Heussinger, Phys. Rev. E **93**, 030901(R) (2016).
[39] R. N. Chacko, R. Mari, M. E. Cates, and S. M. Fielding, Phys. Rev. Lett. **121**, 108003 (2018).
[40] S. Gokhale *et al.*, Proc. Natl. Acad. Sci. USA **109**, 20314 (2012).
[41] S. K. Dutta, A. Mbi, R. C. Arevalo, and D. L. Blair, Rev. Sci. Inst. **84**, 063702 (2013).
[42] A. Kuijk *et al.*, Particle Particle Syst. Character. **31**, 706 (2014).
[43] T. Borzsonyi, B. Szabo, G. Toros, S. Wegner, J. Torok, E. Somfai, T. Bien, and R. Stannarius, Phys. Rev. Lett. **108**, 228302 (2012).
[44] T. Nath and C. Heussinger, arXiv:1812.00757v1.
[45] R. Mari, J. Rheology **64**, 239 (2020).
[46] R. C. Arevalo, P. Kumar, J. S. Urbach, and D. L. Blair, PLoS One **10**, e0118021 (2015).
[47] N. Park, V. Rathee, D. L. Blair, and J. C. Conrad, Phys. Rev. Lett. **122**, 228003 (2019).